DOI: 10.1534/genetics.110.124222

A Link Between Impaired Purine Nucleotide Synthesis and Apoptosis in *Drosophila melanogaster*

Catherine Holland,[1] David B. Lipsett[2] and Denise V. Clark[3]

Department of Biology, University of New Brunswick, Fredericton, New Brunswick E3B 5A3, Canada

Manuscript received October 17, 2010
Accepted for publication March 10, 2011

ABSTRACT

The biosynthetic pathways and multiple functions of purine nucleotides are well known. However, the pathways that respond to alterations in purine nucleotide synthesis *in vivo* in an animal model organism have not been identified. We examined the effects of inhibiting purine *de novo* synthesis *in vivo* and in cultured cells of *Drosophila melanogaster*. The purine *de novo* synthesis gene *ade2* encodes phosphoribosylformylglycinamidine synthase (EC 6.3.5.3). An *ade2* deletion, generated by *P*-element transposon excision, causes lethality in early pupal development, with darkening, or necrosis, of leg and wing imaginal disc tissue upon disc eversion. Together with analysis of a previously isolated weaker allele, *ade2*^{1}, and an allele of the *Prat* gene, which encodes an enzyme for the first step in the pathway, we determined that the lethal arrest and imaginal disc phenotypes involve apoptosis. A transgene expressing the baculovirus caspase inhibitor p35, which suppresses apoptosis caused by other stresses such as DNA damage, suppresses both the imaginal disc tissue darkening and the pupal lethality of all three purine *de novo* synthesis mutants. Furthermore, we showed the presence of apoptosis at the cellular level in both *ade2* and *Prat* mutants by detecting TUNEL-positive nuclei in wing imaginal discs. Purine *de novo* synthesis inhibition was also examined in tissue culture by *ade2* RNA interference followed by analysis of genome-wide changes in transcript levels. Among the upregulated genes was *HtrA2*, which encodes an apoptosis effector and is thus a candidate for initiating apoptosis in response to purine depletion.

THE pathway for *de novo* synthesis of purine nucleotides is almost universal, with exceptions among the intracellular parasites that obtain purines from their host (Chaudhary *et al.* 2004). Thus, although all organisms have pathways for uptake and salvage of purine nucleotides, the *de novo* synthesis pathway is essential. In multicellular organisms, the enzymes for the ten step pathway for synthesis of inosine monophosphate (IMP) are encoded by six genes, where three genes encode polypeptides with multifunctional properties (Figure 1) (Henikoff 1987). IMP is the common precursor for further synthesis to adenosine monophosphate (AMP) and guanosine monophosphate (GMP).

In mammalian tissue culture cell lines, *de novo* synthesis of purines is more active in proliferating cells than in differentiating cells (Natsumeda *et al.* 1984; Barankiewicz and Cohen 1987; Ahmed and Weidemann 1994). As a result, this pathway has been a target for the development of anticancer drugs, including purine analogs such as 6-mercaptopurine and folate antimetabolites such as DDATHF and methotrexate (Christopherson *et al.* 2002). The cellular effects of these drugs likely vary due to their degree of specificity for a particular enzyme. For example, methotrexate targets three enzymes in the purine *de novo* synthesis pathway (Sant *et al.* 1992), whereas DDATHF targets a single enzyme (Christopherson *et al.* 2002). In addition, the effects of inhibitors vary with cell type, leading to death or reversible arrest, depending on the presence or absence of a G_1 checkpoint, respectively (Zhang *et al.* 1998). The inhibition of purine *de novo* synthesis by drug inhibitors leads to growth arrest, or quiescence, possibly through detection of ribonucleotide levels by p53 rather than by DNA damage (Linke *et al.* 1996). However, growth arrest can be independent of p53 status (Bronder and Moran 2002). Thus, the mechanism of growth arrest in mammalian cells caused by purine *de novo* synthesis inhibitors, and its dependence on p53, has not been clearly established.

Two genetic disorders in the purine *de novo* synthesis pathway have been associated with the ADSL (Sivendran *et al.* 2004) and ATIC (Marie *et al.* 2004) genes (Figure 1). In both cases, individuals are short-lived and suffer from profound effects on neurological development.

Supporting information is available online at http://www.genetics.org/cgi/content/full/genetics.110.124222/DC1.

Microarray expression data: NCBI GEO accession GSE24123.

[1]*Present address:* Faculty of Medicine, Dalhousie University, Halifax, NS B3H 4R2, Canada.

[2]*Present address:* Department of Biology, Memorial University, St. John's, NL A1B 3X9, Canada.

[3]*Corresponding author:* Department of Biology, University of New Brunswick, 10 Bailey Dr., Fredericton, NB E3B 5A3, Canada.
E-mail: clarkd@unb.ca

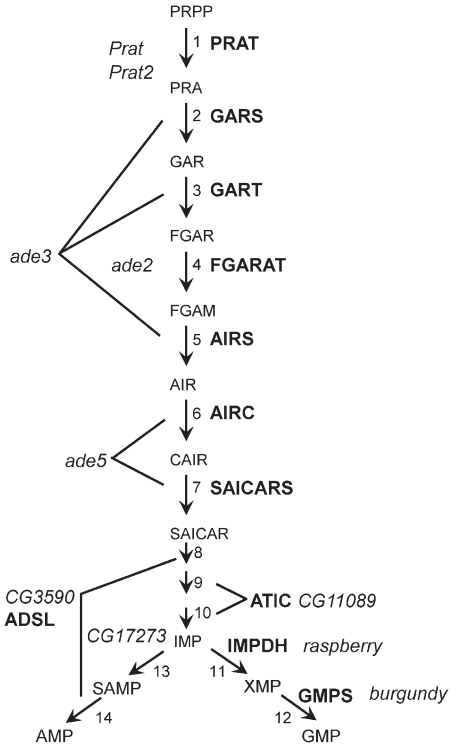

Figure 1.—Purine *de novo* synthesis pathway genes in *D. melanogaster*. Pathway intermediates: PRPP, 5-phosphoribosyl-1-pyrophosphate; PRA, 5-phosphoribosyl-1-amine; GAR, 5-phosphoribosylglycinamide; FGAR, 5-phosphoribosyl *N*-formylglycinamide; FGAM, 5-phosphoribosyl *N*-formylglycinamidine; AIR, 5-phosphoribsylaminoimidazole; CAIR, 5-phosphoribosyl-5-aminoimidazole carboxylate; SAICAR, 5-phosphoribosyl 4-(*N*-succinocarboxamide)-5-aminoimidazole; SAMP, adenylosuccinate; XMP, xanthosine monophosphate. Pathway enzymes: 1—PRAT, phosphoribosylamidotransferase; 2—GARS, GAR synthetase; 3—GART, GAR transformylase; 4—FGARAT, FGAR amidotransferase; 5—AIRS, AIR synthetase; 6—AIRC, AIR carboxylase; 7—SAICARS, SAICAR synthetase; 8 and 14—ADSL, adenylosuccinate lyase; 9 and 10—ATIC, AICAR transformylase-inosinate cyclohydrolase; 11—IMPDH, IMP dehydrogenase; 12—GMPS, GMP synthetase; 13—SAMP synthetase.

Mutations in the other genes in the purine *de novo* synthesis pathway have not been recovered in humans.

Since the cellular and developmental effects of specifically inhibiting purine *de novo* synthesis are not well characterized and would be informative for understanding the mechanisms of drug inhibitors *in vivo*, we are exploring these effects in *Drosophila melanogaster*. Purine *de novo* synthesis gene mutations cause arrest in development from pupal stages to the adult stage with a variety of defects in wing, leg, eye, and bristle development (Tiong *et al.* 1989; Tiong and Nash 1990; Clark 1994; Ji and Clark 2006) as well as reduced fertility and life span (Malmanche and Clark 2004). Here, we focus on identifying factors that respond to depletion of purine *de novo* synthesis during development and in a cell line. We examine mutations in *Prat* and *ade2*, which encode enzymes for the first and fourth steps in the pathway, respectively (Figure 1). Both the pupal lethal arrest of mutants and the necrosis in imaginal tissue can be suppressed by an apoptotic caspase inhibitor. Consistent with these results, an *in situ* cell death assay of wing imaginal discs from newly formed pupae shows apoptotic nuclei. To identify genes responding to purine *de novo* synthesis depletion, we knocked down *ade2* expression in a Drosophila Schneider cell line and performed a gene expression microarray analysis. We identified several genes with up- or down-regulated transcripts, including *HtrA2*, a serine protease associated with apoptosis in Drosophila (Challa *et al.* 2007) and humans (Vande Walle *et al.* 2008).

MATERIALS AND METHODS

Drosophila culture: *D. melanogaster* strains were obtained from the Bloomington Drosophila Stock Center, with the exception of $ade2^4/SM1$ (from David Nash), flies carrying *Df(3R) dsx43* (from Bruce Baker), and $Prat^{12A19}/TM6B$ (from this lab). Flies were cultured on standard cornmeal–molasses–agar medium at 25° and 60% relative humidity. Schneider cell strain #6 (S2) was obtained from the Drosophila Genomics Resource Center and was cultured in Invitrogen Schneider cell medium supplemented with 10% fetal bovine serum at 25°. Cell viability was measured by exclusion of trypan blue, and metabolic activity was measured using the tetrazolium salt WST-1 (Roche Applied Science).

Fly crosses: *P*-element insertion *P{EPgy2}EY05576* (Bellen *et al.* 2004) was used to generate deletions in *ade2* (Voelker *et al.* 1984). Virgin $y\ w^{67c23};\ P\{EPgy2\}EY05576$ females were crossed to $w^{1118};\ al\ b\ c\ sp/CyO;\ ry^{506}\ Dr\ P\{\Delta 2\text{-}3\}99B/TM6B,\ Tb$ males. Dysgenic F_1 $w^{1118};\ P\{EPgy2\}EY05576/al\ b\ c\ sp;\ ry^{506}\ Dr\ P\{\Delta 2\text{-}3\}99B/+$ males were crossed to *w; al b c sp* virgins to identify both *P*-element excision and *P*-element-induced male recombination events (Chen *et al.* 1998) by exchange of the flanking markers *al* and *b*. White-eyed F_2 males of genotype *w; ade2*/al b c sp*, where *ade2** represents a possible excision allele, were crossed to *w; Df(2L)TE35BC-31, b pr pk cn sp/CyO, b** to balance *ade2**, since the *b* marker on *CyO, b** allowed distinction between the two second chromosomes. The resulting *w; ade2*/CyO, b** strains were then screened for absence of *ade2** homozygous adults. Lethal mutations were balanced over the green fluorescent protein (GFP)-marked *CyO, P{GAL4-Kr.C}DC3, P{UAS-GFP.S65T}DC* (*CyO, Kr-GFP*) (Casso *et al.* 2000) to allow identification of mutant homozygotes. A viable excision allele, $ade2^{1-5}$, was also kept. Mutations were mapped to the *ade2* region by complementation test-crosses with *w; Df(2L)ED343/CyO, Kr-GFP* (Ryder *et al.* 2004). Deletion breakpoints were mapped by PCR and sequencing using primers flanking the *P*-element insertion site (Figure 2 and Table S1). A *UAS-ade2* cDNA transgene was constructed by inserting the 4.2-kb *Xba*I partial digest fragment of cDNA GM01721 (Rubin *et al.* 2000) into the *Xba*I site of pUASP (Rorth 1998). Transformants in strain w^{1118} were generated by Genetic Services. cDNA expression was driven by *P{tubP-GAL4}LL7* (Lee and Luo 1999).

For examining p35 suppression, we used chromosome 2- and 3-linked insertions of *P{UAS-p35.H}* (Zhou *et al.* 1997) or *UAS-p35*. For $ade2^{1-6}$ suppression, non-Tubby progeny pupae were scored from three crosses: (1) $ade2^{1-6}$ *; +/CyO:TM6B* siblings, where *CyO:TM6B* is *T(2;3)TSTL, CyO: TM6B, Tb*; (2) $ade2^{1-6}$*; +/CyO:TM6B* crossed to $ade2^{1-6}$*; UAS-p35/CyO:TM6B*; and (3) $ade2^{1-6}$*; UAS-p35/CyO:TM6B* siblings. For $ade2^4$ (Tiong *et al.* 1989) suppression (the $ade2^4$ chromosome

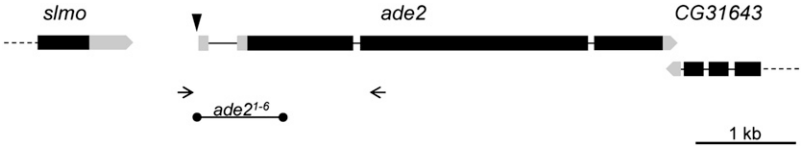

Figure 2.—*P*-element-induced deletion allele *ade2*$^{1-6}$. Map of region containing *ade2* based on Flybase FB2010_06 (June 25, 2010). Thick bars represent exons, with shading indicating untranslated regions and solid indicating coding sequence. Thin lines represent introns. Downward triangle indicates site of *P*-element insertion *P{EPgy2}EY05576* (Bellen *et al.* 2004). Horizontal line under the map shows the extent of the *ade2*$^{1-6}$ deletion. Arrows show the position of primers used to identify and sequence the allele (Figure S1).

carried *P{neoFRT}40A*, which is not relevant in this study), non-Tubby pupae were scored from two crosses: (1) *ade2*^{4}*; +/CyO:TM6B* crossed with *Df(2L)ED343; UAS-p35/CyO:TM6B* and (2) *ade2*^{4}*; +/CyO:TM6B* crossed with *Df(2L)ED343; +/CyO:TM6B*. For *Prat*^{12A19} suppression, non-Tubby pupae were scored from two crosses: (1) *+*; *Prat*^{12A19}*e*^{11}*/TM6B* crossed with *+; Df(3R)dsx43 e*^{11}*/TM6B* and (2) *UAS-p35; Prat*^{12A19} *e*^{11}*/CyO:TM6B* crossed with *+; Df(3R)dsx43 e*^{11}*/TM6B*, where *Df(3R)dsx43* deletes *Prat* and flanking genes (Clark 1994). Non-Tubby stage P1 white prepupae (Bainbridge and Bownes 1981) were also used for detection of *p35* transcripts by RT-PCR. For examining suppression of *ade2*$^{1-6}$ by *p53*$^{5A-1-4}$ (Rong *et al.* 2002), progeny of *ade2*$^{1-6}$*; p53*$^{5A-1-4}$*/CyO:TM6B* siblings and *ade2*$^{1-6}$*; +/CyO:TM6B* siblings were compared. Crosses were set up in parallel with 5 males and either 10 or 20 virgin females in clear polycarbonate vials to allow scoring of undisturbed pupae on sides of vials. Parents were transferred every 24 hr. Time after egg deposition (AED) was measured in days since the transfer. For tests of suppression of necrosis and pupal lethality of the three purine mutants, each group of data was examined by chi-square analysis, and a *P*-value was determined (Preacher 2001). For TUNEL assays and real-time quantitative RT-PCR assays, *ade2*$^{1-5}$and *ade2*$^{1-6}$ homozygous stage P1 white prepupae and third instar wandering larvae were identified in stocks carrying the *CyO, Kr-GFP* balancer chromosome, while *Prat*^{12A19} *e*^{11}*/Df(3R)dsxR43 e*^{11} individuals were generated as described above.

TUNEL assays: TUNEL assays followed Kim *et al.* (2007) with a 100 mm sodium citrate permeabilization step added (Vicente-Crespo *et al.* 2008). Following TUNEL dUTP-FITC labeling (Roche Applied Science), Draq5 nuclear staining (Molecular Probes) was done at 10 μm in PBS with 0.1% Triton-X100 for 30 min. Positive controls for TUNEL labeling were generated by a 1- to 2-hr, 37° heat shock 4–24 hr before dissection (Perez-Garijo *et al.* 2004). The *ade2* experiment was performed on *ade2*$^{1-6}$ and *ade2*$^{1-5}$ discs (with and without heat shock) in parallel, and the *Prat* experiment was performed with *Prat*^{12A19}*e*^{11}*/Df(3R)dsx43 e*^{11} and *e*^{11} discs (with and without heat shock) in parallel. Discs were mounted in 70% glycerol in 1× PBS and imaged using a Leica TCS-SP2 confocal microscope. *Z*-series of images were collected using the average intensity setting, and channels were merged using ImageJ (Abramoff *et al.* 2004).

RNA interference in tissue culture cells: To control for possible off-target effects using double-stranded RNA (dsRNA) (Ma *et al.* 2006), two non-overlapping templates were prepared using the *ade2* cDNA LD23935 (Rubin *et al.* 2000). The *ade2* dsRNA-1 template was a 741-bp *Sac*I–*Hin*dIII fragment cloned into both pSPT18 and pSPT19 vectors (Roche Applied Science) to allow synthesis of complementary single-stranded RNA (ssRNA). The *ade2* dsRNA-2 template was made by PCR using the T7 primer and 5′-GGGGATCCAAATCGTAGTCGTT GAAGG-3′ to produce a 745-bp product and then digested with *Eco*RI and *Bam*HI and cloned into pSPT18 and pSPT19. A nonspecific dsRNA was made from a Chlamydomonas *lhcb* cDNA 313-bp *Bgl*II–*Pst*I fragment (GenBank accession AY171229) kindly provided by D. Durnford. Complementary ssRNAs were made using linearized templates and a T7 polymerase transcription kit (Ambion), followed by annealing. Treatment of Drosophila S2 cells with dsRNA was done in triplicate for 4 days at 25° with 30 μg dsRNA/ml of cells at an initial density of 1×10^6 (Maiato *et al.* 2003).

Microarray hybridization: RNA was extracted from S2 cells using Trizol (Invitrogen). Each replicate represents cells treated and grown in a separate dish. Three replicates of each of the *ade2* dsRNA-1 and *lhcb* dsRNA treatments and two replicates of the *ade2* dsRNA-2 treatment underwent RNA labeling, hybridization using the Agilent 1-color protocol, microarray scanning, and data normalization at the Laboratory for Advanced Genome Analysis at the Vancouver Prostate Centre, Vancouver, Canada, as follows. RNA was linearly amplified and labeled with Cy3, and labeled cRNA quantity and specific activity were assessed with the NanoDrop ND-1000 (Thermo Scientific, Wilmington, DE). Labeled cRNA (1.65 μg) was fragmented for 30 min and applied to Agilent Drosophila microarrays in the 4 × 44,000 format (product G2519F), hybridized for 17 hr at 65° in the Agilent hybridization oven, and washed with Agilent wash buffers. Scanning was done with the Agilent DNA Microarray Scanner at a 5-μm resolution. Agilent's Feature Extraction 9.1 software was used for background subtraction and quality control measurements. The intensities per spot had their local background subtracted. A step of spatial detrending was done using the negative control spots across the whole array and subtracting a surface fit from the data. The data were loaded into GeneSpring 7.3, and raw values <5 were set to 5. The data were normalized to the median, so that intensities were divided by the median of all intensities. Normalized and raw data were deposited in the GEO database at NCBI (accession GSE24123). A *t*-test *P*-value for significance of each value above background was calculated. For comparison among microarrays, mean values for each treatment were used in a *t*-test comparing expression levels between treatments, and a fold-change value for the corresponding spot was calculated. Normalized values were flagged as A (absent) or P (present or marginal), and these flags were used for filtering the data into different classes for production of gene lists.

Western blots: A polyclonal anti-Ade2 antiserum (Alpha Diagnostic International) was raised in rats against a recombinant Ade2 polypeptide. A 776-bp *Bam*HI–*Xho*I fragment from the 3′-end of the LD23935 cDNA (Rubin *et al.* 2000) was inserted into pQE30 (Qiagen), producing a 219-amino-acid 6X-His protein. The antiserum was affinity-purified against 6XHis-Ade2 as previously described (Gu *et al.* 1994; Clark and Macafee 2000). Western blot detection was done using the Aurora blocking reagent and protocol (MP Biomedicals) with alkaline phosphatase (AP)-conjugated donkey anti-rat IgG (Jackson Immunoresearch) secondary antibody. α-Tubulin was detected using mouse antibody DM1A (Sigma) and AP-conjugated goat anti-mouse IgG (Sigma). AP was detected using CDP-Star (New England Biolabs). Images were captured on X-ray film and digitally scanned.

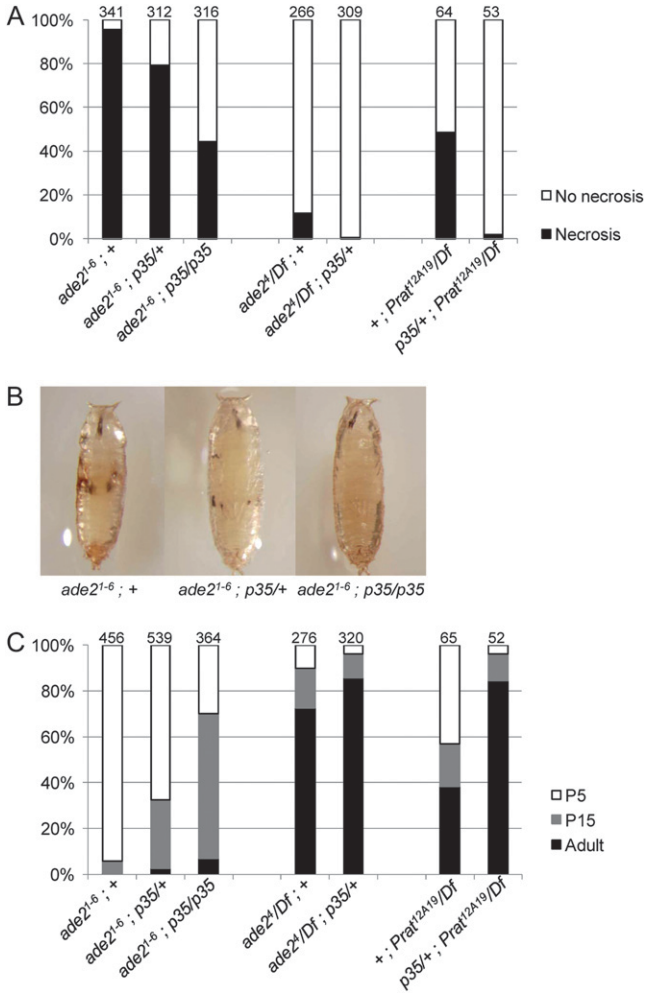

Figure 3.—Suppression of *ade2* and *Prat* mutant phenotypes by baculovirus protein p35. (A) Presence of necrosis at pupal stage P5 (Bainbridge and Bownes 1981) and older, scored at 7 days AED for $ade2^{1-6}$ and 9 days AED for $ade2^{4}$ and $Prat^{12A19}$. Numbers at the top indicate total pupae scored for each genotype. (B) Representative P5 individuals for the three $ade2^{1-6}$ genotypes scored in A. (C) Proportions surviving to pupal stages P5, P15, and adult. Numbers at top indicate total pupae/adults scored. Chi-square analyses for groups of data for each mutant, for both A and C, gave *P*-values ≤0.0001.

Quantitative RT-PCR: *ade2* mRNA levels were checked in the RNA samples used for microarrays by quantitative reverse transcription PCR (qRT-PCR) using a Superscript III Platinum SYBR green two-step kit with ROX and the Applied Biosystems 7900HT instrument. *ade2* RNA levels were normalized to *ribosomal protein 49* (*rp49*) levels.

For qRT-PCR analysis of genes showing differential expression in the microarray, primers were designed using either AUTOPRIME version 1.0 (Wrobel *et al.* 2004) or Primer3 (Rozen and Skaletsky 2000) if the gene lacked introns (Table S1). RNA was treated with RQ1 DNAse (Promega). cDNA synthesis and qRT-PCR were done using a Superscript III Platinum Two-Step qRT-PCR kit with SYBR Green (Invitrogen) and a Rotor-Gene 6000 (Corbett Life Science). Amplification conditions were 95° for 2 min and then 40 cycles of 95° for 15 sec, 60° for 30 sec, and 72° for 30 sec, followed by ramping from 72° to 95° for melt curve analysis. Each reaction was done in triplicate along with a negative control produced without reverse transcriptase. Rotor-Gene data were exported to LinReg Version 12.5 (Ruijter *et al.* 2009) to determine primer efficiency and C_T values and then to REST Version 2.0.13 (Pfaffl *et al.* 2002) to calculate fold changes in RNA levels between *ade2* RNA interference (RNAi) and the *lhcb* control. The RNA for the gene of interest was normalized to *rp49* RNA levels in each sample.

RESULTS

Generation of an *ade2* deletion by *P*-element excision: The *P*-element insertion *P{EPgy2}EY05576* (Bellen *et al.* 2004) maps 19 bp upstream from the 5′-end of the *ade2-RA* and *ade2-RB* transcripts (Tweedie *et al.* 2009) (Figure 2). Of 30 independent excisions, $ade2^{1-6}$ and $ade2^{3-20}$ showed pupal lethality. Analysis of $ade2^{1-6}$ genomic DNA showed an 856-bp deletion starting from the site of the *P*-element insertion and extending into the *ade2*-coding region (Figure S1). A total of 33 bp of *P*-element inverted repeat sequence remain at the insertion site, and the sequence upstream of the insertion site is intact. This deletion removes the predicted transcription start sites and 393 bp of coding sequence. A *UAS-ade2* transgene, driven by ubiquitously expressed *tub-GAL4*, is sufficient to rescue the pupal lethality of $ade2^{1-6}$, and the rescued adults appear wild-type (Figure S2). Sequence analysis of the viable $ade2^{1-5}$ allele showed that it had a wild-type sequence (Tweedie *et al.* 2009) and thus was the result of a precise *P*-element excision (data not shown).

Purine syndrome phenotype is suppressed by expression of baculovirus protein p35: The purine syndrome phenotype shows pupal lethality or adult escapers with wing and leg phenotypes indicating defects in cell proliferation (Tiong *et al.* 1989). The most severe *ade2* alleles show arrest predominantly at pupal stage P5 with characteristic darkened tissue, or "necrotic" regions, in the everted wing and leg imaginal discs (Ji and Clark 2006). This phenotype is also found for *Prat* mutants (Clark 1994; Ji and Clark 2006). To determine whether the developmental arrest and necrotic tissues are associated with apoptosis, we tested the ability of the baculovirus protein p35 (Hay *et al.* 1994) to suppress these phenotypes.

Flies with an $ade2^{1-6}$, $ade2^{4}$, or $Prat^{12A19}$ mutation and a p35-expressing transgene were compared to the same mutants not carrying the p35 transgene. *UAS-p35* is normally used with a GAL4 driver (Phelps and Brand 1998); however, during the process of strain construction, we noted that the *UAS-p35* transgene was sufficient to suppress the purine syndrome phenotype alone in the absence of a GAL4 driver (Figure 3). Both the P5 arrest and the necrosis were suppressed in both *ade2* mutants. In addition, the degree of suppression with one copy of the *UAS-p35* transgene was less than that for two copies. The necrosis and lethal arrest found for the $ade2^{4}$ and $Prat^{12A19}$ hemizygous mutants were also suppressed by one copy of *UAS-p35* inserted on

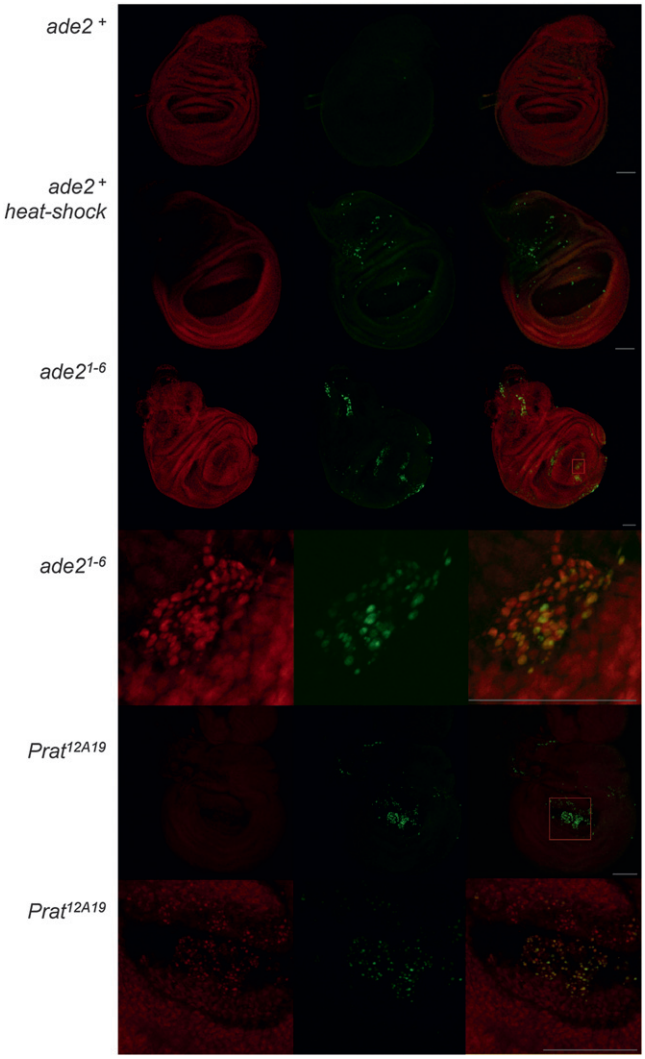

FIGURE 4.—Apoptosis as measured by TUNEL assays in wing imaginal discs of *ade2* and *Prat* mutants. Genotypes of wing discs in each row are indicated at left. Sets of three images are, from left to right: Draq5 nuclear stain, TUNEL FITC stain, and an overlay of the two images. For the *ade2* and *Prat* mutant discs, higher resolution images of each red-box region, highlighting a group of TUNEL-positive nuclei, are shown. Scale bar, 50 μm.

chromosomes 3 and 2, respectively. Therefore, the suppression of the purine syndrome phenotype by *UAS-p35* is not specific to a particular *ade2* allele; nor is it specific to a particular *UAS-p35* transgene insert or purine *de novo* synthesis gene.

Since a GAL4 driver was not used to induce *UAS-p35* expression, we wanted to verify that the *UAS-p35* transgene was expressed in the absence of a GAL4 driver. RT-PCR assays for p35 transcripts were done for $ade2^{1-6}$; *UAS-p35* pupae and for $ade2^{1-6}$; *UAS-p35* and *UAS-p35*; $Prat^{12A19}$/*Df(3R)dsx43* stage P1 prepupal wing discs. Results showed that the *p35* transgene is indeed transcribed in the absence of a GAL4 driver for both genotypes (Figure S3). Therefore, the developmental arrest and the necrotic phenotype found for the purine syndrome phenotype in *ade2* and *Prat* mutants are dependent on the caspase activity suppressed by p35.

Since the transcription factor p53 can be an effector in the apoptotic response to DNA damage (LU and ABRAMS 2006), we tested the ability of a null mutation in *p53*, $p53^{5A\text{-}1\text{-}4}$ (RONG *et al.* 2002), to suppress the necrosis in stage P5-arrested pupae. We found no significant difference in the degree of necrosis between $ade2^{1-6}$; $p53^{5A\text{-}1\text{-}4}$ and $ade2^{1-6}$; + pupae (Figure S4A). The *reaper*, *hid*, and *grim* genes are apoptosis effectors that antagonize the inhibitor of apoptosis protein DIAP1, allowing activation of caspases (XU *et al.* 2009), and these genes map to a region uncovered by the deficiency *Df(3L)H99* (WHITE *et al.* 1994). *H99* heterozygotes show a reduction in apoptosis in wing imaginal discs of irradiated larvae (BRODSKY *et al.* 2004). Thus, we asked whether the necrosis in $ade2^{1-6}$ stage P5-arrested pupae was suppressed in a *H99*/+ genetic background. We found no significant difference in the degree of necrosis in this genetic background (Figure S4B).

Apoptosis is detected in *ade2* and *Prat* mutant wing imaginal discs of white prepupae: To determine if the *ade2* and *Prat* mutant phenotypes are associated with apoptosis at the cellular level, we examined wing imaginal discs for DNA strand breaks using the TUNEL assay. We found that wing discs from white prepupae for both $ade2^{1-6}$ homozygotes ($n = 6$) and $Prat^{12A19}$ e^{11}/*Df(3R)dsxR43* e^{11} heterozygotes ($n = 6$) showed TUNEL-positive nuclei, particularly over the wing pouch region (Figure 4). We also noted that the TUNEL-positive nuclei were smaller and more condensed than the surrounding nuclei, as is found with apoptotic nuclei (DENTON *et al.* 2008).

Gene expression response to knockdown of *ade2* expression in S2 tissue culture cells: To examine the gene expression response to a reduction in purine *de novo* nucleotide synthesis, we generated two non-overlapping *ade2* dsRNAs (dsRNA-1 and dsRNA-2) to knock down expression of *ade2* in Drosophila S2 tissue culture cells and observed the genome-wide changes in transcript abundance using microarray hybridization. We verified that our *ade2* dsRNA knockdown by both non-overlapping dsRNAs was affecting expression of *ade2* protein by Western blot analysis (Figure S5A). Growth and metabolic activity of *ade2* dsRNA-treated cells were reduced, as measured by WST-1 assay (Figure S5B). Changes in transcript abundance were measured relative to a Chlamydomonas *lhcb* dsRNA. A total of 198 and 210 microarray probes showed significantly different hybridization signals for *ade2* dsRNA-1 *vs. lhcb* and *ade2* dsRNA-2 *vs. lhcb* treatments, respectively, and 41 probes were common to both comparisons. A candidate list was compiled for the 20 genes showing absolute values of $\log_2$ fold changes ≥ 0.9 (Table S2).

We examined expression of the 20 genes for changes in transcript levels by qRT-PCR. One biological replicate was examined for each of the *ade2* dsRNA-1, *ade2*

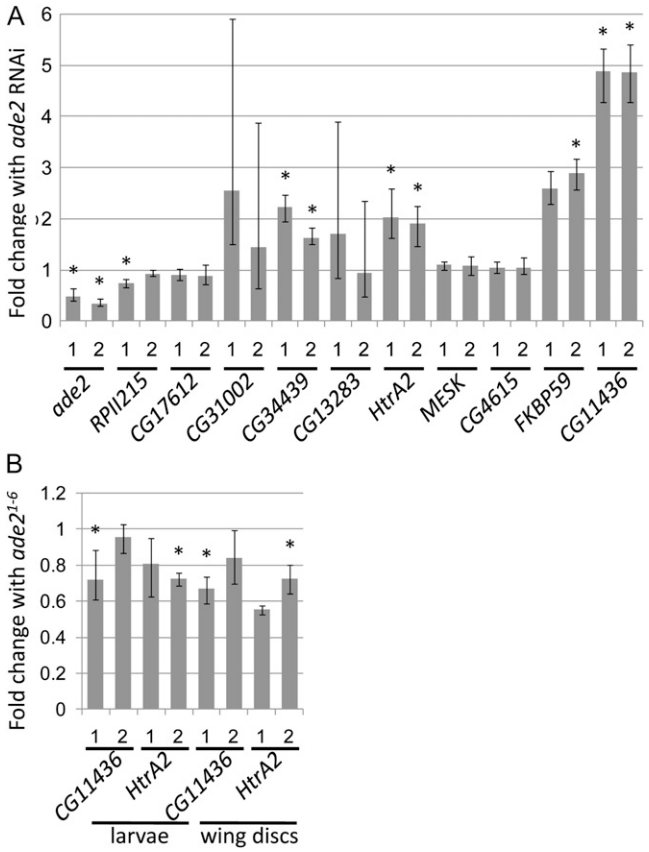

Figure 5.—Genes that respond to *ade2* RNAi in tissue culture cells. (A) Fold changes in transcript levels measured by qRT-PCR in cells treated with *ade2* dsRNA-1 and *ade2* dsRNA-2 relative to cells treated with control *lhcb* dsRNA. (B) Fold changes in transcript levels measured by qRT-PCR in whole wandering third instar larvae and stage P1 prepupal wing discs. Error bars show standard errors of fold changes, and asterisks show results where the probability of a type 1 error P(H1) is <0.05, as calculated by the REST program (Pfaffl *et al.* 2002).

dsRNA-2, and control *lhcb* dsRNA treatments. Transcripts from 9 genes (*CG6660*, *CG3649*, *CG5866*, *DNAseII*, *CG41436*, *CG5773*, *Pph13*, *CG14432*, and *Ank2*) could not be detected by qRT-PCR either at all or sufficiently in any sample to reliably measure fold changes. The data for the 11 other genes are shown in Figure 5A. Interpro domain (Hunter *et al.* 2009) and microarray data are summarized in Table 1. As expected, *ade2* showed significantly reduced transcript levels. Five genes (*RPII215*, *CG34439*, *HtrA2*, *FKBP59*, and *CG11436*) showed reproducible fold changes in response to *ade2* RNAi in comparison to the microarray data. The other 5 genes showed no significant change in expression; however, for the genes *CG31002* and *CG13283*, results were unreliable, primarily due to low transcript abundance and C_T values >35.

Two *ade2* RNAi-responsive genes were further explored *in vivo*. We selected *CG11436* because it showed the greatest response to *ade2* RNAi and *HtrA2* because it is associated with a pro-apoptotic function. For $ade2^{1-6}$ in comparison to $ade2^{1-5}$, in both whole wandering third instar larvae and dissected stage P1 prepupal wing discs, we found a slight reduction in expression of both genes (Figure 5B). Therefore, both *CG11436* and *HtrA2* are responsive to *ade2* loss of function *in vivo*, but in an opposite direction in comparison to S2 cells.

DISCUSSION

Depletion of purine *de novo* synthesis causes darkened tissue to develop in pupal imaginal tissue at the P5 stage when imaginal disc eversion has occurred. This darkened tissue, or necrosis, for lack of a better term, is suppressed by the caspase inhibitor *p35*. Furthermore, *p35* expression improves survival through metamorphosis. Thus, it appears that purine depletion at this stage of development causes a caspase-dependent cell death in imaginal discs and perhaps elsewhere. Examination of wing imaginal discs from white prepupae, before disc eversion, shows compact TUNEL-positive nuclei. We do not know whether these nuclei directly correspond to the necrotic tissue seen after disc eversion; however, the TUNEL-positive nuclei cluster in the center of the wing pouch, which becomes the distal portion of the wing after disc eversion, where we see necrosis along with the distal regions of the legs.

The term "necrosis" is being used here to describe the darkening tissue that we observe in early pupal development. It is not being used to classify the phenomenon as the caspase-independent cellular response that is often markedly distinguished from apoptosis (Edinger and Thompson 2004; Harwood *et al.* 2005), although non-overlapping classification of different types of cell death can be difficult (Broker *et al.* 2005). Darkening of imaginal tissue has also been referred to as melanization, in an effort to classify tissues undergoing an immune response mediated by hemocytes, known as melanotic masses (Minakhina and Steward 2006). Mutations in genes associated with apoptosis, such as *dcp-1*, show a gut melanization phenotype that is not typical of an immune response. There is no hemocyte encapsulation and tissue overgrowth typical of melanotic masses (Minakhina and Steward 2006). It is likely that the darkened "necrotic" tissue that we observe is similar to the melanization seen with mutations in genes such as *dcp-1*.

The folate antimetabolites methotrexate and aminopterin inhibit dihydrofolate reductase (DHFR), which is required for both purine and pyrimidine *de novo* synthesis in addition to serine, glycine, and methionine synthesis (McGuire 2003). These drugs appear to have quite different effects compared to mutations in purine *de novo* synthesis genes. For example, methotrexate causes melanotic tumors in larvae, in addition to affecting ovarian, wing, and leg development (Affleck and Walker 2007). Aminopterin causes a notched wing phenotype (Legent *et al.* 2006) that is distinct from that

TABLE 1

Genes showing changes in transcript levels in response to *ade2* RNA interference in S2 cells that were also assayed by real-time qRT-PCR

Gene	Interpro domain[a]	Log_2 fold change[b]	*P*-value
ade2	IPR010073: Phosphoribosylformylglycinamidine synthase	−2.56	0.000
RpII215	IPR000722: RNA polymerase, α-subunit	−2.01	0.011
CG17612	IPR007087: Zinc finger, C2H2-type	−1.09	0.025
CG31002	IPR002213: UDP-glucuronosyl/UDP-glucosyltransferase	0.88	0.044
CG34439	Unknown	0.91	0.004
		0.93	0.007
CG13283	IPR000718: Peptidase M13, neprilysin	0.94	0.004
HtrA2	IPR009003: Peptidase cysteine/serine, trypsin-like	1.09	0.001
MESK2	IPR004142: Ndr family (*N*-myc-downstream-repressed)	1.10	0.009
CG4615	IPR004254: Hly-III-related (hemolysin III-related)	1.13	0.004
FKBP59	IPR001179: Peptidyl-prolyl *cis-trans* isomerase, FKBP-type	1.35	0.001
CG11436	IPR013026: Tetratricopeptide repeat-containing	2.05	0.000
		2.44	0.001

[a]Interpro domain (Hunter *et al.* 2009) was reported in FlyBase (Tweedie *et al.* 2009). In cases where several domains are reported, one functionally descriptive entry was selected.
[b]Log_2 fold change absolute values ≥0.9 as detected by microarray analysis. Transcripts showing two values correspond to the values for two different oligonucleotides on the microarray. See Table S2 for details.

for *ade2* (Tiong *et al.* 1989) and *Prat* (Clark 1994) mutants. Interestingly, apoptosis in wing discs caused by aminopterin can be suppressed by overexpression of the nucleotide salvage enzyme deoxyribonucleotide kinase (Legent *et al.* 2006), despite the multiple roles of DHFR.

Both *Prat* and *Prat2* encode the same enzyme yet are essential genes with distinctive pupal lethal phenotypes. Simultaneous RNAi knockdown of both genes gives a phenotype similar to the *ade2* mutant phenotype (Ji and Clark 2006). In wandering third instar larvae, *Prat* is expressed in imaginal discs, whereas *Prat2* is expressed in the fat body (Penney *et al.* 2008). *ade2* is expressed throughout development, including in the larval fat body (Chintapalli *et al.* 2007). Since we saw strong suppression of the *Prat* mutant phenotype, we suspect that the suppression is occurring directly by expression of *p35* in imaginal discs, rather than through an indirect effect such as suppression of a fat body disorder due to purine depletion.

The expression of the *UAS-p35* transgene without a GAL4 driver was sufficient to suppress *ade2* and *Prat* mutants. We presume that expression of the *UAS-p35* transgene is either due to activation of the trangene promoter by flanking enhancer elements or due to a basal level of transcription that is simply a property of this particular construction (Zhou *et al.* 1997). We are not aware of a previous study detecting expression of *UAS-p35* alone, as the numerous studies documented in FlyBase that used *UAS-p35* all used a GAL4 driver (Tweedie *et al.* 2009).

We did not see suppression of $ade2^{1-6}$ by a *p53* mutation. p53 is a transcription factor that effects apoptosis in response to radiation-induced DNA damage (Brodsky *et al.* 2004). There is some evidence for a latent response to DNA damage that is caspase-dependent but independent of *p53* (Wichmann *et al.* 2006); however, the factors involved in detecting this response have not been identified. Drosophila Myc appears to be an alternative sensor to DNA damage caused by radiation (Montero *et al.* 2008). Thus, it is possible that the reduction in purine *de novo* synthesis is detected through a p53-independent pathway. Mammalian cell culture studies have equivocal findings as to whether p53 is also involved in detection of reduced nucleotide pools to elicit a G_o/G_1 arrest (Linke *et al.* 1996; Bronder and Moran 2002).

We also did not see a significant suppression of $ade2^{1-6}$ in heterozygotes for the *H99* deficiency of the *reaper*, *hid*, and *grim* gene region (White *et al.* 1994). The reduced dosage of these effector genes can suppress the apoptosis response to radiation-induced DNA damage (Brodsky *et al.* 2004). Therefore, our finding suggests that the caspase-dependent response that we observe may be dependent on a different apoptosis effector. Alternatively, the reduced dosage of the apopotic effector genes may simply not have been sufficient to suppress the response to a block in purine *de novo* synthesis.

Our gene expression analysis of S2 cells with reduced *ade2* expression revealed a small set of genes with changes in transcript levels. We likely have several false negatives due to subtle effects, since the cells were cultured in media that was not depleted of purines. However, these conditions are likely to reflect situations *in vivo* where purines are available from the diet or from cellular turnover. *HtrA2* attracted our interest as it has been quite extensively characterized with respect to a role in stress response and apoptosis. *HtrA2* encodes a serine protease that is localized to the mitochondrial intermembrane space (Challa *et al.* 2007). It is released when the outer mitochondrial membrane is

permeabilized in response to stress that leads to inhibition of the inhibitor of apoptosis protein DIAP1, as shown in S2 cells. However, others have shown that *HtrA2* is not necessary for apoptosis *in vivo*, as there is a normal apoptotic response to gamma radiation in wing imaginal discs in *HtrA2* mutants (Tain *et al.* 2009). *HtrA2* mutants are viable, but they show male sterility and reduced stress resistance and longevity (Yun *et al.* 2008; Tain *et al.* 2009). We found a reproducible twofold increase in *HtrA2* transcripts in response to *ade2* knockdown in S2 cells. However, this increase was not found in $ade2^{1-6}$ mutant third instar larvae or in stage P1 prepupal wing discs; rather, we observed a weak decrease. Therefore, expression of *HtrA2* in response to depletion of purine *de novo* synthesis needs to be explored further.

In conclusion, we have found a link between depletion of purine nucleotide synthesis and apoptosis *in vivo*. Whether purine nucleotide levels are sensed directly, or indirectly through a cellular stress response, remains to be determined. However, we found no clear evidence for involvement of *p53* or the apoptosis effectors *reaper, hid*, and *grim*. Further analysis of the roles of other known members of apoptotic pathways, including *HtrA2*, and the other genes that we found responsive to *ade2* knockdown, will be an important next step in the analysis of this response.

The authors acknowledge Sharon Gorski, Douglas Freeman, and the British Columbia Genome Sciences Centre for generously providing expertise and facilities for developing gene expression knockdown in tissue culture cells. We also acknowledge Anne Haegert and Robert Bell of the Laboratory for Advanced Genome Analysis at the Vancouver Prostate Centre, Vancouver, Canada, for carrying out the Agilent microarray hybridization and data analysis. We thank Nancy Macafee for anti-ade2 antibody purification. Microscopy was conducted with technical help from Susan Belfry of the Microscopy and Microanalysis Facility at the University of New Brunswick. This work was supported by a McCain Visitorship and Canadian Institutes of Health Research, New Brunswick Health Research Foundation, and New Brunswick Innovation Foundation grants to D.V.C.

LITERATURE CITED

Abramoff, M. D., P. J. Magelhaes and S. J. Ram, 2004 Image processing with ImageJ. Biophotonics International **11:** 36–42.

Affleck, J. G., and V. K. Walker, 2007 Transgenic rescue of methotrexate-induced teratogenicity in Drosophila melanogaster. Toxicol. Sci. **99:** 522–531.

Ahmed, N., and M. J. Weidemann, 1994 Purine metabolism in promyelocytic HL60 and dimethylsulphoxide-differentiated HL60 cells. Leuk. Res. **18:** 441–451.

Bainbridge, S. P., and M. Bownes, 1981 Staging the metamorphosis of *Drosophila melanogaster*. J. Embryol. Exp. Morphol. **66:** 57–80.

Barankiewicz, J., and A. Cohen, 1987 Purine nucleotide metabolism in phytohemagglutinin-induced human T lymphocytes. Arch. Biochem. Biophys. **258:** 167–175.

Bellen, H. J., R. W. Levis, G. Liao, Y. He, J. W. Carlson *et al.*, 2004 The BDGP gene disruption project: single transposon insertions associated with 40% of Drosophila genes. Genetics **167:** 761–781.

Brodsky, M. H., B. T. Weinert, G. Tsang, Y. S. Rong, N. M. McGinnis *et al.*, 2004 Drosophila melanogaster MNK/Chk2 and p53 regulate multiple DNA repair and apoptotic pathways following DNA damage. Mol. Cell. Biol. **24:** 1219–1231.

Broker, L. E., F. A. Kruyt and G. Giaccone, 2005 Cell death independent of caspases: a review. Clin. Cancer Res. **11:** 3155–3162.

Bronder, J. L., and R. G. Moran, 2002 Antifolates targeting purine synthesis allow entry of tumor cells into S phase regardless of p53 function. Cancer Res. **62:** 5236–5241.

Casso, D., F. Ramirez-Weber and T. B. Kornberg, 2000 GFP-tagged balancer chromosomes for Drosophila melanogaster. Mech. Dev. **91:** 451–454.

Challa, M., S. Malladi, B. J. Pellock, D. Dresnek, S. Varadarajan *et al.*, 2007 Drosophila Omi, a mitochondrial-localized IAP antagonist and proapoptotic serine protease. EMBO J. **26:** 3144–3156.

Chaudhary, K., J. A. Darling, L. M. Fohl, W. J. Sullivan Jr., R. G. Donald *et al.*, 2004 Purine salvage pathways in the apicomplexan parasite Toxoplasma gondii. J. Biol. Chem. **279:** 31221–31227.

Chen, B., T. Chu, E. Harms, J. P. Gergen and S. Strickland, 1998 Mapping of Drosophila mutations using site-specific male recombination. Genetics **149:** 157–163.

Chintapalli, V. R., J. Wang and J. A. Dow, 2007 Using FlyAtlas to identify better Drosophila melanogaster models of human disease. Nat. Genet. **39:** 715–720.

Christopherson, R. I., S. D. Lyons and P. K. Wilson, 2002 Inhibitors of de novo nucleotide biosynthesis as drugs. Acc. Chem. Res. **35:** 961–971.

Clark, D. V., 1994 Molecular and genetic analyses of Drosophila *Prat*, which encodes the first enzyme of *de novo* purine biosynthesis. Genetics **136:** 547–557.

Clark, D. V., and N. MacAfee, 2000 The purine biosynthesis enzyme PRAT detected in proenzyme and mature forms during development of *Drosophila melanogaster*. Insect Biochem. Mol. Biol. **30:** 315–323.

Denton, D., K. Mills and S. Kumar, 2008 Methods and protocols for studying cell death in Drosophila. Methods Enzymol. **446:** 17–37.

Edinger, A. L., and C. B. Thompson, 2004 Death by design: apoptosis, necrosis and autophagy. Curr. Opin. Cell Biol. **16:** 663–669.

Gu, J., C. G. Stephenson and M. J. Iadarola, 1994 Recombinant proteins attached to a Nickel-NTA column: use in affinity purification of antibodies. Biotechniques **17:** 257–261.

Harwood, S. M., M. M. Yaqoob and D. A. Allen, 2005 Caspase and calpain function in cell death: bridging the gap between apoptosis and necrosis. Ann. Clin. Biochem. **42:** 415–431.

Hay, B. A., T. Wolff and G. M. Rubin, 1994 Expression of baculovirus P35 prevents cell death in Drosophila. Development **120:** 2121–2129.

Henikoff, S., 1987 Multifunctional polypeptides for purine *de novo* synthesis. BioEssays **6:** 8–13.

Hunter, S., R. Apweiler, T. K. Attwood, A. Bairoch, A. Bateman *et al.*, 2009 InterPro: the integrative protein signature database. Nucleic Acids Res. **37:** D211–D215.

Ji, Y., and D. V. Clark, 2006 The purine synthesis gene *Prat2* is required for Drosophila metamorphosis, as revealed by inverted-repeat-mediated RNA interference. Genetics **172:** 1621–1631.

Kim, H. J., S. H. Kim, S. O. Shim, E. Park, C. Kim *et al.*, 2007 Drosophila homolog of APP-BP1 (dAPP-BP1) interacts antagonistically with APPL during Drosophila development. Cell Death Differ. **14:** 103–115.

Lee, T., and L. Luo, 1999 Mosaic analysis with a repressible cell marker for studies of gene function in neuronal morphogenesis. Neuron **22:** 451–461.

Legent, K., M. Mas, A. Dutriaux, S. Bertrandy, D. Flagiello *et al.*, 2006 In vivo analysis of Drosophila deoxyribonucleoside kinase function in cell cycle, cell survival and anti-cancer drugs resistance. Cell Cycle **5:** 740–749.

Linke, S. P., K. C. Clarkin, A. Di Leonardo, A. Tsou and G. M. Wahl, 1996 A reversible, p53-dependent G0/G1 cell cycle arrest induced by ribonucleotide depletion in the absence of detectable DNA damage. Genes Dev. **10:** 934–947.

Lu, W. J., and J. M. Abrams, 2006 Lessons from p53 in non-mammalian models. Cell Death Differ. **13:** 909–912.

Ma, Y., A. Creanga, L. Lum and P. A. Beachy, 2006 Prevalence of off-target effects in Drosophila RNA interference screens. Nature **443:** 359–363.

Maiato, H., C. E. Sunkel and W. C. Earnshaw, 2003 Dissecting mitosis by RNAi in Drosophila tissue culture cells. Biol. Proced. Online **5:** 153–161.

Malmanche, N., and D. V. Clark, 2004 *Drosophila melanogaster Prat*, a purine *de novo* synthesis gene, has a pleiotropic maternal effect phenotype. Genetics **168:** 2011–2023.

Marie, S., B. Heron, P. Bitoun, T. Timmerman, G. Van Den Berghe *et al.*, 2004 AICA-ribosiduria: a novel, neurologically devastating inborn error of purine biosynthesis caused by mutation of ATIC. Am. J. Hum. Genet. **74:** 1276–1281.

McGuire, J. J., 2003 Anticancer antifolates: current status and future directions. Curr. Pharm. Des. **9:** 2593–2613.

Minakhina, S., and R. Steward, 2006 Melanotic mutants in Drosophila: pathways and phenotypes. Genetics **174:** 253–263.

Montero, L., N. Muller and P. Gallant, 2008 Induction of apoptosis by Drosophila Myc. Genesis **46:** 104–111.

Natsumeda, Y., N. Prajda, J. P. Donohue, J. L. Glover and G. Weber, 1984 Enzymic capacities of purine *de novo* and salvage pathways for nucleotide synthesis in normal and neoplastic tissues. Cancer Res. **44:** 2475–2479.

Penney, J., J. Bosse and D. V. Clark, 2008 Expression pattern diversity and functional conservation between retroposed PRAT genes from Drosophila melanogaster and Drosophila virilis. J. Mol. Evol. **66:** 457–471.

Perez-Garijo, A., F. A. Martin and G. Morata, 2004 Caspase inhibition during apoptosis causes abnormal signalling and developmental aberrations in Drosophila. Development **131:** 5591–5598.

Pfaffl, M. W., G. W. Horgan and L. Dempfle, 2002 Relative expression software tool (REST) for group-wise comparison and statistical analysis of relative expression results in real-time PCR. Nucleic Acids Res. **30:** e36.

Phelps, C. B., and A. H. Brand, 1998 Ectopic gene expression in *Drosophila* using GAL4 system, pp. 367–379 in *METHODS: A Companion to Methods in Enzymology*, Vol. 14. Academic Press, New York.

Preacher, K. J., 2001 Calculation for the chi-square test: an interactive calculation tool for chi-square tests of goodness of fit and independence. http://www.quantpsy.org.

Rong, Y. S., S. W. Titen, H. B. Xie, M. M. Golic, M. Bastiani *et al.*, 2002 Targeted mutagenesis by homologous recombination in D. melanogaster. Genes Dev. **16:** 1568–1581.

Rorth, P., 1998 Gal4 in the Drosophila female germline. Mech. Dev. **78:** 113–118.

Rozen, S., and H. J. Skaletsky, 2000 Primer3 on the WWW for general users and for biologist programmers, pp. 365–386 in *Bioinformatics Methods and Protocols: Methods in Molecular Biology*, edited by S. Krawetz and S. Misener. Humana Press, Totowa, NJ. http:/http://frodo.wi.mit.edu/primer3.

Rubin, G. M., L. Hong, P. Brokstein, M. Evans-Holm, E. Frise *et al.*, 2000 A Drosophila complementary DNA resource. Science **287:** 2222–2224.

Ruijter, J. M., C. Ramakers, W. M. Hoogaars, Y. Karlen, O. Bakker *et al.*, 2009 Amplification efficiency: linking baseline and bias in the analysis of quantitative PCR data. Nucleic Acids Res. **37:** e45.

Ryder, E., F. Blows, M. Ashburner, R. Bautista-Llacer, D. Coulson *et al.*, 2004 The DrosDel collection: a set of *P*-element insertions for generating custom chromosomal aberrations in *Drosophila melanogaster*. Genetics **167:** 797–813.

Sant, M. E., S. D. Lyons, L. Phillips and R. I. Christopherson, 1992 Antifolates induce inhibition of amido phosphoribosyltransferase in leukemia cells. J. Biol. Chem. **267:** 11038–11045.

Sivendran, S., D. Patterson, E. Spiegel, I. McGown, D. Cowley *et al.*, 2004 Two novel mutant human adenylosuccinate lyases (ASLs) associated with autism and characterization of the equivalent mutant Bacillus subtilis ASL. J. Biol. Chem. **279:** 53789–53797.

Tain, L. S., R. B. Chowdhury, R. N. Tao, H. Plun-Favreau, N. Moisoi *et al.*, 2009 Drosophila HtrA2 is dispensable for apoptosis but acts downstream of PINK1 independently from Parkin. Cell Death Differ. **16:** 1118–1125.

Tiong, S. Y. K., and D. Nash, 1990 Genetic analysis of the *adenosine3* (*Gart*) region of the second chromosome of *Drosophila melanogaster*. Genetics **124:** 889–897.

Tiong, S. Y. K., C. Keizer, D. Nash and D. Patterson, 1989 Drosophila purine auxotrophy: new alleles of *adenosine2* exhibiting a complex visible phenotype. Biochem. Genet. **27:** 333–348.

Tweedie, S., M. Ashburner, K. Falls, P. Leyland, P. McQuilton *et al.*, 2009 FlyBase: enhancing Drosophila Gene Ontology annotations. Nucleic Acids Res. **37:** D555–D559.

Vande Walle, L., M. Lamkanfi and P. Vandenabeele, 2008 The mitochondrial serine protease HtrA2/Omi: an overview. Cell Death Differ. **15:** 453–460.

Vicente-Crespo, M., M. Pascual, J. M. Fernandez-Costa, A. Garcia-Lopez, L. Monferrer *et al.*, 2008 Drosophila muscleblind is involved in troponin T alternative splicing and apoptosis. PLoS One **3:** e1613.

Voelker, R. A., A. L. Greenleaf, H. Gyurkovics, G. B. Wisely, S. M. Huang *et al.*, 1984 Frequent imprecise excision among reversions of a *P* element-caused lethal mutation in Drosophila. Genetics **107:** 279–294.

White, K., M. E. Grether, J. M. Abrams, L. Young, K. Farrell *et al.*, 1994 Genetic control of programmed cell death in Drosophila. Science **264:** 677–683.

Wichmann, A., B. Jaklevic and T. T. Su, 2006 Ionizing radiation induces caspase-dependent but Chk2- and p53-independent cell death in Drosophila melanogaster. Proc. Natl. Acad. Sci. USA **103:** 9952–9957.

Wrobel, G., F. Kokocinski and P. Lichter, 2004 AutoPrime: selecting primers for expressed sequences. Genome Biol. **5:** 1–7.

Xu, D., S. E. Woodfield, T. V. Lee, Y. Fan, C. Antonio *et al.*, 2009 Genetic control of programmed cell death (apoptosis) in Drosophila. Fly (Austin) **3:** 78–90.

Yun, J., J. H. Cao, M. W. Dodson, I. E. Clark, P. Kapahi *et al.*, 2008 Loss-of-function analysis suggests that Omi/HtrA2 is not an essential component of the PINK1/PARKIN pathway in vivo. J. Neurosci. **28:** 14500–14510.

Zhang, C. C., T. J. Boritzki and R. C. Jackson, 1998 An inhibitor of glycinamide ribonucleotide formyltransferase is selectively cytotoxic to cells that lack a functional G1 checkpoint. Cancer Chemother. Pharmacol. **41:** 223–228.

Zhou, L., A. Schnitzler, J. Agapite, L. M. Schwartz, H. Steller *et al.*, 1997 Cooperative functions of the reaper and head involution defective genes in the programmed cell death of Drosophila central nervous system midline cells. Proc. Natl. Acad. Sci. USA **94:** 5131–5136.

Communicating editor: M. Wolfner

GENETICS

Supporting Information
http://www.genetics.org/cgi/content/full/genetics.110.124222/DC1

A Link Between Impaired Purine Nucleotide Synthesis and Apoptosis in *Drosophila melanogaster*

Catherine Holland, David B. Lipsett and Denise V. Clark

DOI: 10.1534/genetics.110.124222

FIGURE S1.—Sequenced region of *ade2*[16]. Triangle = EY05576 insertion site as reported in Genbank accession BZ748943.1, Upper case = mRNA sequence, Lower case = intergenic sequence and introns, Lower case and underlined = partial sequence of a P-element inverted repeat, Red font = *ade2* CDS, Yellow highlight = sequence deleted in *ade2*[16].

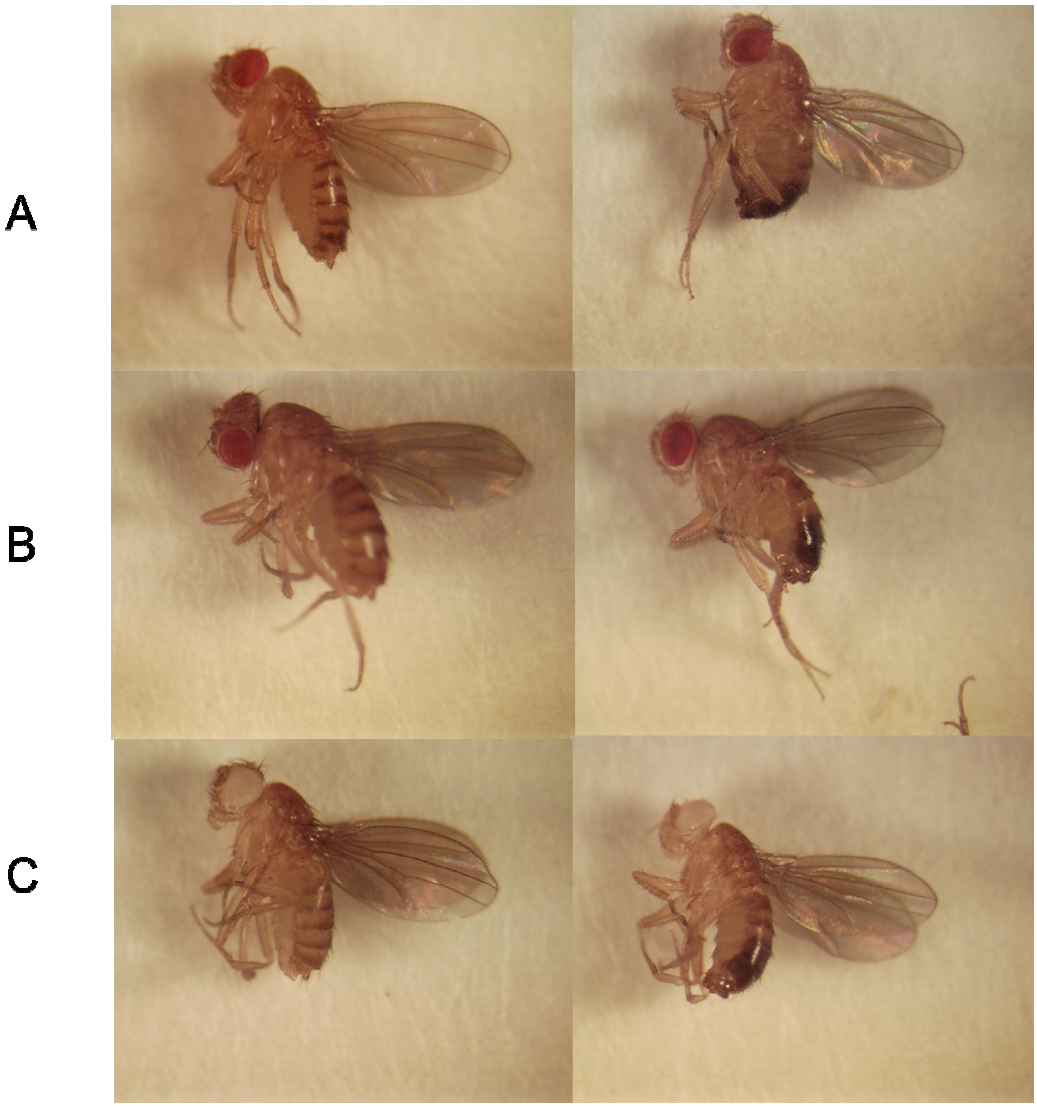

FIGURE S2.—Rescue of *ade2*$^{-}$ by expression of an *ade2* cDNA transgene. A) *ade2*$^{-}$*; UAS-ade2cDNA[1-28-1]/tub-GAL4* female (left) and male (right), B) Canton S wild-type female (left) and male (right), C) *ade2*$^{-}$ (wild-type excision) homozygous female (left) and male (right).

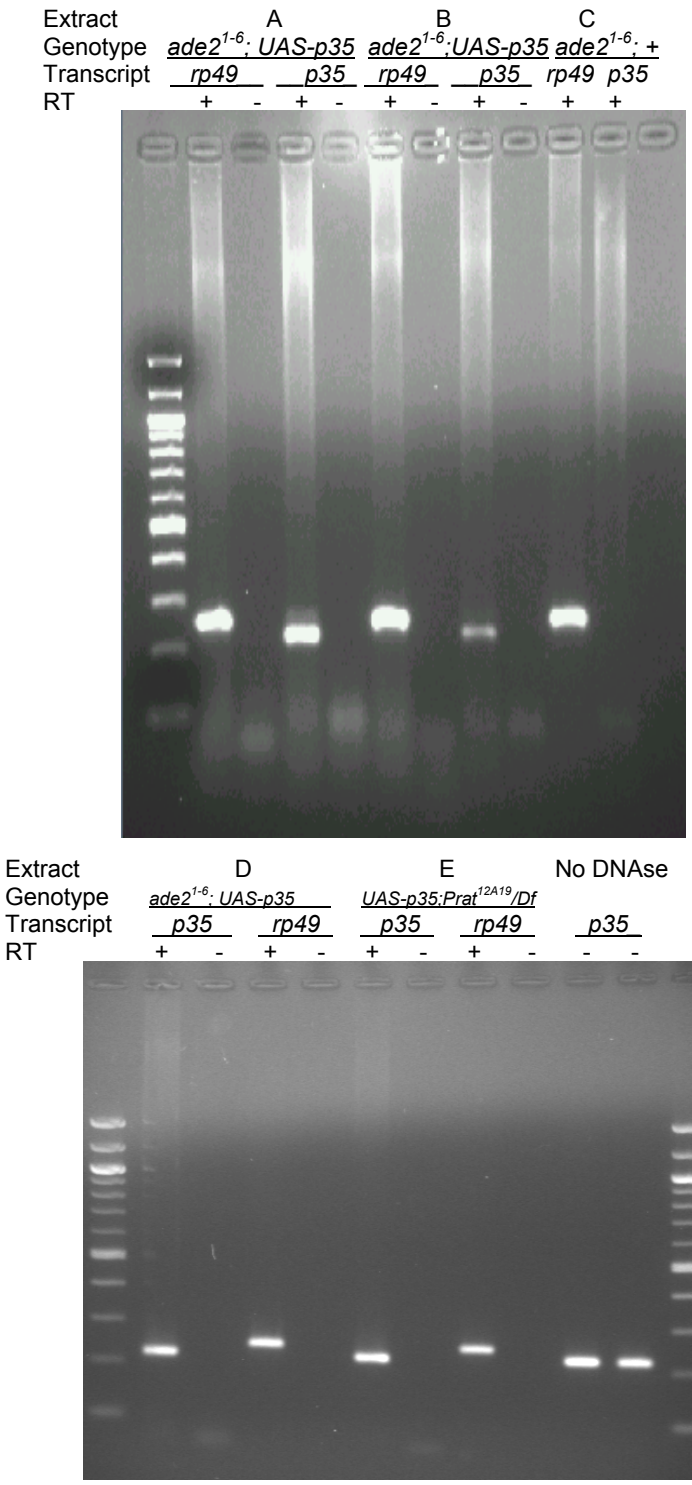

FIGURE S3.—RT-PCR detection of *p35* transcripts in *UAS-p35* transgenic flies in the absence of a GAL4 driver. Five RNA extractions were performed: A and B) 2 groups of *ade2*$^{1-6}$*; UAS-p35* pupae from independent vials, C)*ade2*$^{1-6}$ pupae, D) *ade2*$^{1-6}$*; UAS-p35* stage P1 puparium wing imaginal discs, and E) *UAS-p35 ; Prat*^{12A19}*/Df(3R)dsx43* stage P1 puparium wing imaginal discs using Trizol as directed (Invitrogen). Reverse transcription was performed using the cDNA synthesis component of the 2-step qRT-PCR kit with SYBR (Invitrogen) and PCR was done using standard *Taq* polymerase and reagents (New England Biolabs). The "No DNAse" lanes show PCR products generated on extracts D and E prior to DNAse treatment, showing the products generated from genomic DNA. Primers are listed in Table S1. M=100 bp DNA ladder (New England Biolabs).

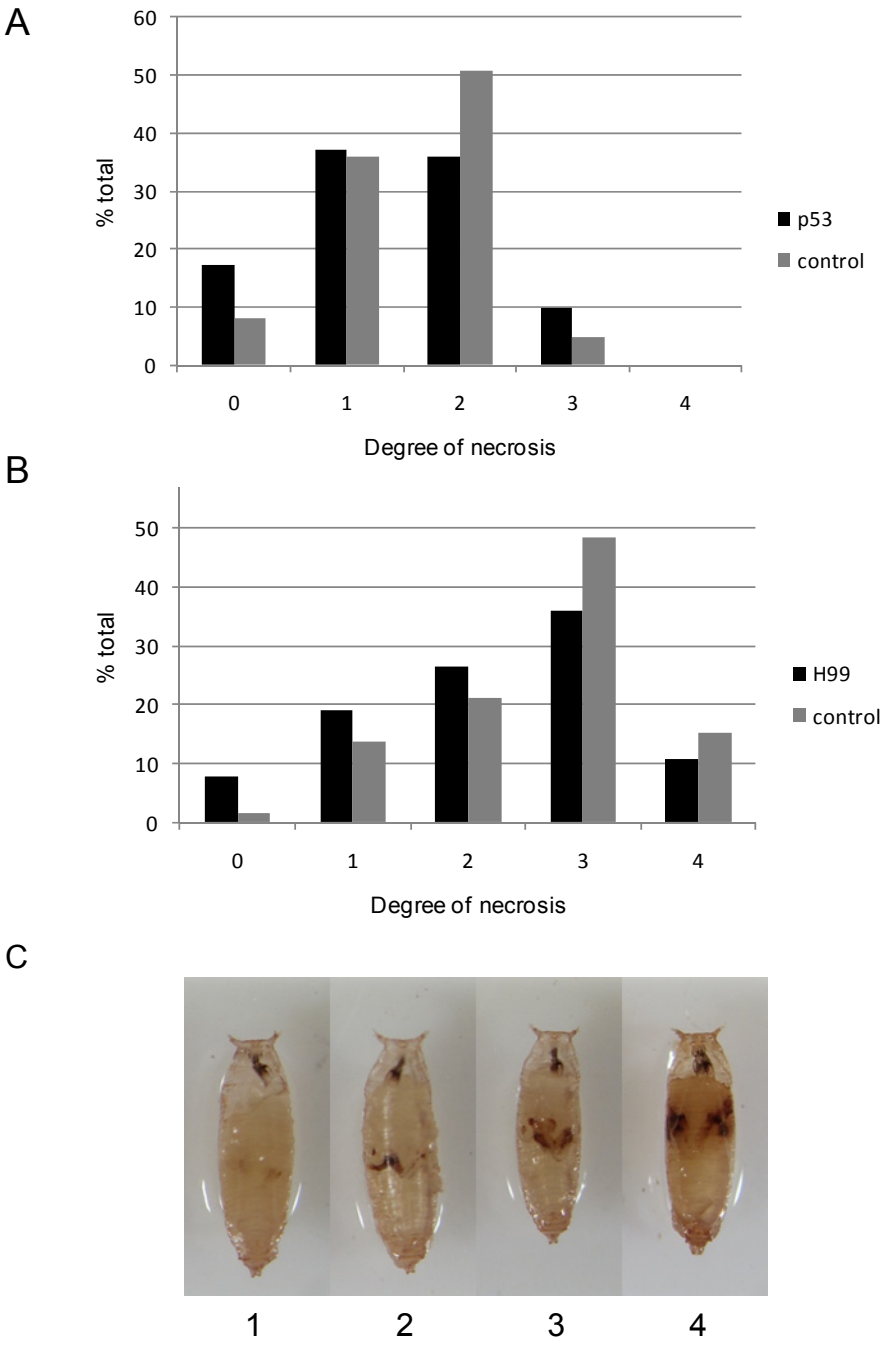

FIGURE S4.—Test for suppression of *ade2*^{1} by a *p53* null mutation and by the *reaper, hid, grim* deletion *H99/+*. A) *ade2*^{1} *; p53*$^{5A-1-4}$ (n=81) versus *ade2*^{1} *; +* (n=61) P5 pupae. Chi-squared analysis gave p = 0.16 at x^2 = 5.118 and 3df (3df since no class 4 pupae were scored). B) *ade2*^{1} *; Df(3L)H99/TM2* (n=167) versus *ade2*^{1}*; +* (n=66) P5 pupae. Chi-squared analysis gave a p value of 0.13 at x^2 = 7.058 and 4df. C) Degree of darkened tissue, or necrosis, for each stage P5 pupa was scored qualitatively as one of 5 classes, where 0=no necrosis and representative classes 1-4 are shown in the photographs.

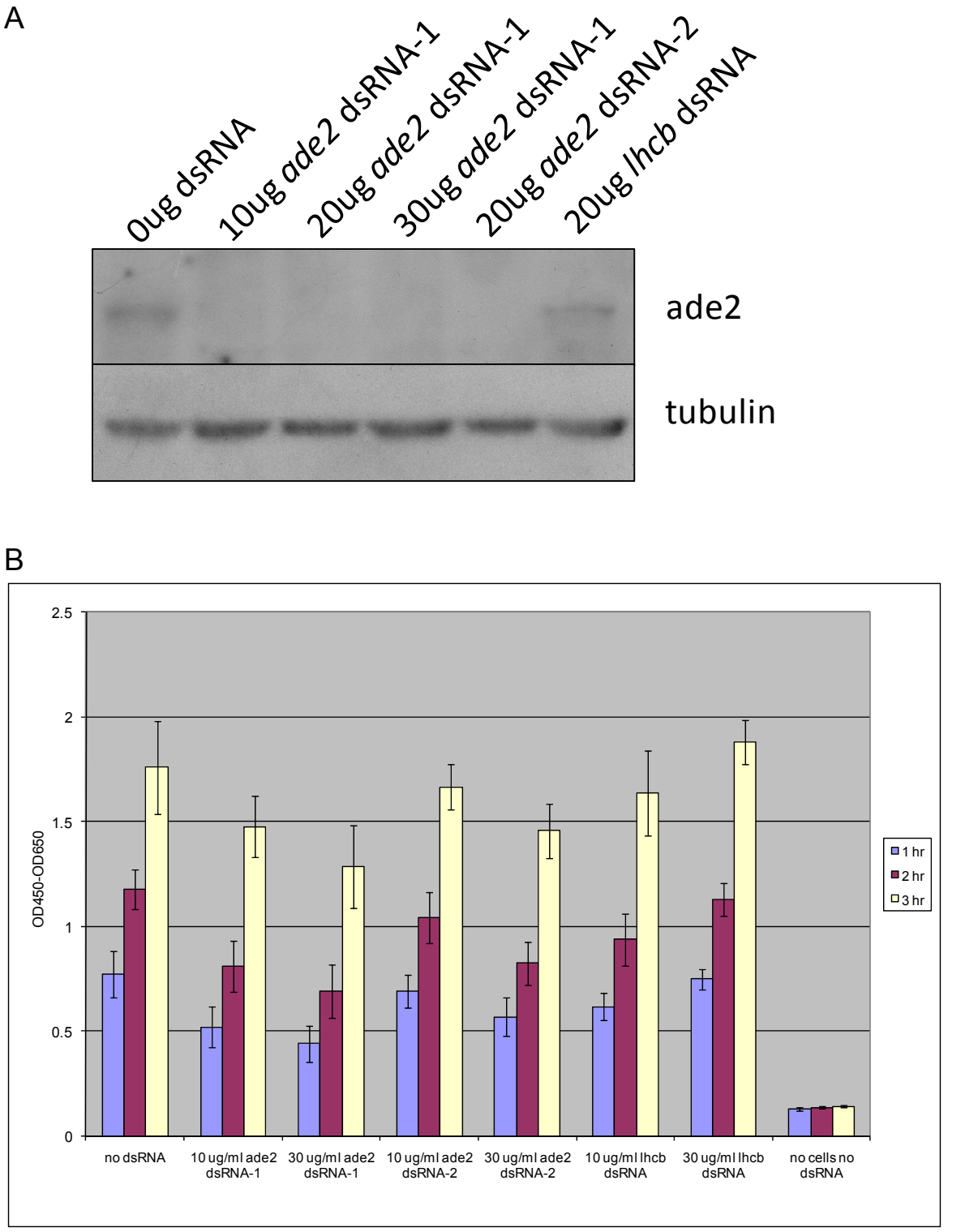

FIGURE S5.—Analysis of S2 cells following treatment with *ade2* dsRNAs and control *Chlamydomonas lhcb* dsRNA. A) Western blot analysis of ade2 expression; B) Cell metabolic activity 4 days after dsRNA treatment was measured by WST-1 assays, as recommended by Roche Life Sciences. OD measurements were taken at 3 time points. Each dsRNA treatment represents 4 replicates; error bars represent +/- SEM.

TABLE S1

Primers used in this study

Primer	Sequence
A) *ade2* P element excision allele analysis	
ade2_for	CCTTGCAAGTTACGCAATGG
ade2_rev2	TGAACATGATCGGTTTCACG
B) p35 RTPCR analysis	
p34_for	AGCGATCAAATGGATGGATTCCACG
p35_rev	CGGCTTCAACACGCATACCGC
CG7939_rp49 L	CTA AGC TGT CGC ACA AAT GG
CG7939_rp49 R	AAT CTC CTT GCG CTT CTT G
C) qRT-PCR analysis of genes identified in microarray experiment	
CG6660L	CCTGAGCAACACCTACCTC
CG6660R	CAGCACTATGAATACCGTGTC
CG6660newL	CTCGACACGGTATTCATAGTG
CG6660newR	AATGAGGCGGCATAGTAGTAG
CG6660L-2	TGCACACGGTGATGTATGC
CG6660R-2	CTGAATGAAGCCGATGAAGG
CG3649L	GTAACCAAAGAGTCGGATCG
CG3649R	CTTTGGTGATGCTTCTGTTTC
ade2 1 F	TCAGCTATGCGGACACTTTG
ade 2 1 R	CATCTTGACGACGCTTGAAA
RpII215L	CCCAGGTTATTGCTTGTGTG
RpII215R	CCCATAGCGTGGAAATAGAAC
CG5866-3L	GAGACACATCGGTCATCACG
CG5866-3R	CAGAAAAAGAAAACAATACAACTTAGG
DNaseIIL	AATGCGATCTCTGTGCTTC
DNaseIIR	TAAAGGTGCCACCAATCTAC

CG41436L	GAACACCAGGAGCCGAATAG
CG41436R	CCTGTGCCTGTGTATCGTTG
CG17612-5L	CGATGGAGAACGTGTGTCAG
CG17612-5R	CCGTCTTCGCCGTTTATG
CG17612Lnew	ATTTGGCACCAAGCATAAGG
CG17612Rnew	TGCTCGCTCCTATGATCTCC
CG5773L	ACACAGTGGCTTGTGCTCAG
CG5773R	CACCGCCATTATTGCATTC
Pph13L	ACTACTCGCCACCCACTC
Pph13R	TGTTAAATGTGGTTCTGTATCTCC
CG31002L	TTTAATGAGGTCCTTAGGATTG
CG31002R	TCGTTATTCAGCACTGTCTTC
CG34439L	ATGATCGGCAATGCTTTC
CG34439R	CTCCTCCTTCTTCACCTCTTC
CG13283-3L	CGAAAAGGCCATGAATCC
CG13283-3R	TTTAAAGTTGAAAACATCAAGTATGTG
CG14332-3L	ATCATCAGCAAATGACCAAAC
CG14332-3R	TTCCGATAGAAAAAGGTTTGAGAG
HtrA2L	GCGCACAGTGGTGGACTC
HtrA2R	AGGGATCTTCTGGCGTAATG
MESK2-2L	ACGGAAAGCGTCAGAAAC
MESK-2R	CGCTTGATTTCTGATTTATTTG
CG4615L	TTACTCACGGCATTTGGATAC
CG4615R	CATTCTTCGGTGGTTTGTG
Ank2-3L	CGGGATTAGGAGAGAGAAAGAG
Ank2-3-R	AGAAGAGCGCCTTGTCTAGC
Ank2Lnew	TGTGCTAGGCGTTGTAATGG
Ank2Rnew	TGTGCTAGGCGTTGTAATGG
FKBP59L	ACGACAAAGAGACCGAACC

FKBP59R	TTCGTATAAGCATTAAGACCATTTC
CG11436L	GACATTGATGTGCTGGAACG
CG11436R	TGCTTTGTGAAGGGAATGTG
CG7939_rp49 L	CTAAGCTGTCGCACAAATGG
CG7939_rp49 R	AATCTCCTTGCGCTTCTTG

[a]Multiiple primer pairs were tested for the genes for which transcripts were not measurable by qRT-PCR due to very low abundance or no detection.

TABLE S2

Fold changes in transcript levels in response to *ade2* RNA interference from microarray hybridization experiment

Gene[a]	Agilent microarray oligonucleotide	Fold change	$\log_2$ fold change	P value
CG6660	A_09_P070456	0.05	-4.20	0.000
CG3649	A_09_P026666	0.14	-2.85	0.001
ade2	A_09_P041166	0.17	-2.56	0.000
RpII215	A_09_P198715	0.25	-2.01	0.011
CG5866	A_09_P148430	0.35	-1.54	0.006
DNAseII	A_09_P042026	0.41	-1.30	0.021
CG41436	A_09_P002781	0.44	-1.18	0.040
CG17612	A_09_P226290	0.47	-1.09	0.025
CG5773	A_09_P220660	0.49	-1.04	0.016
Pph13R	A_09_P076436	0.52	-0.95	0.026
CG31002	A_09_P058696	1.84	0.88	0.044
CG34439	A_09_P004456	1.88	0.91	0.004
	A_09_P004461	1.90	0.93	0.007
CG13283	A_09_P112105	1.92	0.94	0.004
CG14332	A_09_P111835	2.01	1.00	0.013
	A_09_P193290	2.01	1.01	0.023
HtrA2	A_09_P075046	2.13	1.09	0.001
MESK2	A_09_P221410	2.14	1.10	0.009
CG4615	A_09_P189280	2.19	1.13	0.004
Ank2	A_09_P004301	2.25	1.17	0.034
FKBP59	A_09_P066556	2.54	1.35	0.001
CG11436	A_09_P197240	4.13	2.05	0.000
	A_09_P067026	5.42	2.44	0.001

[a] 20 genes, in addition to *ade2*, that responded to *ade2* RNA interference using both *ade2* dsRNA-1 and dsRNA-2 and showed >= 0.9 |$\log_2$ fold change|. One gene, *CG5237*, met the filtering criteria but is not shown because the microarray probe corresponded to an intron sequence.